

Crystal Structure and Physical Properties of Conducting Molecular Antiferromagnets with a Halogen-Substituted Donor: (EDO-TTFBr₂)₂FeX₄ (X = Cl, Br)

A. Miyazaki,^{*,†} H. Yamazaki,[†] M. Aimatsu,[†] T. Enoki,[†] R. Watanabe,[‡] E. Ogura,[‡] Y. Kuwatani,[‡] and M. Iyoda[‡]

Department of Chemistry, Tokyo Institute of Technology, O-okayama, Meguro-ku, Tokyo 152-8551, Japan, and Department of Chemistry, Tokyo Metropolitan University, Minami-Ohsawa, Hachioji, Tokyo 192-0397, Japan

Received September 29, 2006

The crystal structure and physical properties of radical ion salts (EDO-TTFBr₂)₂FeX₄ (X = Cl, Br) based on halogen-substituted organic donor and magnetic anions are investigated, including the comparison with the isomorphous compounds (EDO-TTFBr₂)₂GaX₄ with nonmagnetic anions. The crystal structure of these four salts consists of uniformly stacked donor molecules and tetrahedral counter anions, and the Br substituents of the donor molecules are connected to halide ligands of anions with remarkably short intermolecular atomic distances. These salts show metallic behavior around room temperature and undergo a spin-density-wave transition in the low-temperature range, as confirmed with the divergence of the electron spin resonance (ESR) line width. Although close anion–anion contacts are absent in these salts, the FeCl₄ salt undergoes an antiferromagnetic transition at $T_N = 4.2$ K, and the FeBr₄ salt shows successive magnetic transitions at $T_N = 13.5$ K and $T_{C2} = 8.5$ K with a helical spin structure as a candidate for the ground state of the d-electron spins. The magnetoresistance of the FeCl₄ salt shows stepwise anomalies, which are explained qualitatively using a π –d interaction-based frustrated spin system model composed of the donor π -electron and the anion d-electron spins. Although on the ESR spectra of the FeX₄ salts signals from the π - and d-electron spins are separately observed, the line width of the π -electron spins broadens under the temperature where the susceptibility deviates from the Curie–Weiss behavior, showing the presence of the π –d interaction.

Introduction

The development of molecular solids with two or more different physical properties, such as electron transport and magnetism, is one of the important targets in the field of molecule-based solid-state physics and chemistry.^{1–3} The strategy currently used for developing conducting molecular magnets is to hybridize two components such as an organic molecular conducting layer and a transition-metal magnetic layer. When magnetic ions with d-electrons are introduced as a counterpart for organic donors with π -electrons, an exchange interaction referred to as π –d exchange interaction

works between the donors and anions to realize novel magnetic systems. On the basis of this strategy, a number of molecular antiferromagnets using TTF-type derivatives have been developed, and their electronic and magnetic properties have been investigated in detail.^{4–9} One of the most representative and successful π –d interaction-based

* To whom correspondence should be addressed. E-mail: miyazaki.a.aa@m.titech.ac.jp.

[†] Tokyo Institute of Technology.

[‡] Tokyo Metropolitan University.

(1) Enoki, T.; Miyazaki, A. *Chem. Rev.* **2004**, 5449–5477.

(2) Ouahab, L.; Enoki, T. *Eur. J. Inorg. Chem.* **2004**, 933–941.

(3) Coronado, E.; Day, P. *Chem. Rev.* **2004**, 5419–5448.

(4) Miyazaki, A.; Okabe, K.; Enomoto, K.; Nishijo, J.; Enoki, T.; Setifi, F.; Golhen, S.; Ouahab, L.; Toita, T.; Yamada, J. *Polyhedron* **2003**, 22, 2227–2234.

(5) Miyazaki, A.; Enomoto, K.; Okabe, K.; Yamazaki, H.; Nishijo, J.; Enoki, T.; Ogura, E.; Ugawa, K.; Kuwatani, Y.; Iyoda, M. *J. Solid State Chem.* **2002**, 168, 547–562.

(6) Okabe, K.; Yamaura, J.-I.; Miyazaki, A.; Enoki, T. *J. Phys. Soc. Jpn.* **2005**, 74, 1508–1520.

(7) Enomoto, K.; Yamaura, J.-I.; Miyazaki, A.; Enoki, T. *Bull. Chem. Soc. Jpn.* **2003**, 76, 945–953.

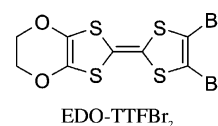
(8) Hanasaki, N.; Tajima, H.; Matsuda, M.; Naito, T.; Inabe, T. *Phys. Rev. B* **2000**, 62, 5839–5842.

(9) Coronado, E.; Galán-Mascarós, J. R.; Gomez-García, C. J.; Laukhin, V. *Nature* **2000**, 408, 447–449.

molecular conducting magnets is λ -(BETS)₂MCl₄ (BETS = bis(ethylenedithio)tetraselenafulvalene, M = Fe, Ga).^{10–14} In this salt the strong π -d exchange interaction, whose magnitude is estimated at 3.7 K by an empirical calculation,¹⁵ enables a π -d coupled antiferromagnetic state and field-induced superconductivity.^{16–19} Besides this exceptional case, the magnitude of the π -d interaction for currently reported conducting magnets is weak and estimated as at most 1 K.¹⁵ One possible reason for the weakness of the π -d interaction is because the interaction path usually relies upon the van der Waals (vdW) interaction between the chalcogen atoms of the donor layer and halogen atoms of the anion layer.

Here we adopt intermolecular halogen...halogen contacts for the purpose of achieving stronger π -d exchange interaction. The presence of an attractive interaction between the halogen substituents is regarded as an electrostatic Coulomb interaction and partial charge transfer. The geometrical preference of the contacts,²⁰ however, is understood as the result of the anisotropic interaction from the lone-pair electron density of the halogen atoms; i.e., the donation of the lone-pair electrons from one halogen atom to the others gives the anisotropy of the interaction. This sort of intermolecular interaction is also observed between halogen atoms and chalcogen or nitrogen atoms, specially referred to as "halogen bonds"^{21,22} in analogy with hydrogen bonds. Due to the geometrical preference of these interactions, radical ion salts using halogen-substituted donor molecules have been investigated mainly from the viewpoint of crystal engineering.^{23–28} Since this mechanism is regarded as that of weak covalent character between two atoms, the

Chart 1



halogen...halogen contacts are also expected to mediate exchange interaction between the conduction π -electrons on the donors and localized d-electrons on the anions.^{29–32} On the basis of this viewpoint, we have recently reported that (EDT-TTFBr₂)₂FeBr₄ (EDT-TTFBr₂ = 4,5-dibromo-4',5'-ethylenedithiotetrathiafulvalene) undergoes an antiferromagnetic transition of the anion d-spins at $T_N = 11$ K, which is significantly high despite its long anion-anion Br-Br contact, suggesting the importance of the π -d interaction in the magnetism.³³ The effect of the π -d interaction in this salt is also featured with negative magnetoresistance that reaches -23% at the highest magnetic field investigated ($B = 15$ T). The mechanism of this phenomenon is explained by the stabilization of the insulating state of the electrons by the periodic magnetic potential of the anion d-spins, which is modified by applying the external magnetic field.

In this work we focused on the oxygen-substituted analogue EDO-TTFBr₂ (4,5-dibromo-4',5'-ethylenedioxytetrathiafulvalene, Chart 1)³⁴ as a donor molecule and FeX₄⁻ (X = Cl, Br) as a magnetic d-anion of molecular conducting antiferromagnets.^{35–37} Using this molecule or its iodine-substituted derivative, we have already reported the coexistence of metallic conduction and ferromagnetic interaction in (EDO-TTFI₂)₂[M(mnt)₂] (M = Ni, Pt; mnt = maleonitriledithiolate)³⁸ and an anomalous metallic state having both itinerant and localized character of the π -electron system in (EDO-TTFBr₂)₃I₃.³⁹ This donor molecule is therefore promising in the development of a molecular conducting magnet with remarkable physical properties. As for the magnetic part, we have been using FeX₄⁻ anions for the following reasons. These anions are stable monovalent anions having large spin quantum numbers ($S = 5/2$). In addition, the use of GaX₄⁻, having no localized spins, helps us to elucidate the role of

- (10) Kobayashi, H.; Cui, H.-B.; Kobayashi, A. *Chem. Rev.* **2004**, *104*, 5265–5288.
- (11) Kobayashi, H.; Kobayashi, A.; Cassoux, P. *Chem. Soc. Rev.* **2000**, *29*, 325–333.
- (12) Kobayashi, H.; Tomita, H.; Naito, T.; Kobayashi, A.; Sakai, F.; Watanabe, T.; Cassoux, P. *J. Am. Chem. Soc.* **1996**, *118*, 368–377.
- (13) Kobayashi, A.; Udagawa, T.; Tomita, H.; Naito, T.; Kobayashi, H. *Chem. Lett.* **1993**, *22*, 2179–2182.
- (14) Kobayashi, H.; Sato, A.; Arai, E.; Akutsu, H. *J. Am. Chem. Soc.* **1997**, *119*, 12392–12393.
- (15) Mori, T.; Katsuhara, M. *J. Phys. Soc. Jpn.* **2002**, *71*, 826–844.
- (16) Uji, S.; Shinagawa, H.; Terashima, T.; Yakabe, T.; Terai, Y.; Tokumoto, M.; Kobayashi, A.; Tanaka, H.; Kobayashi, H. *Nature* **2001**, *410*, 908–910.
- (17) Balicas, L.; Brooks, J. S.; Storr, K.; Uji, S.; Tokumoto, M.; Tanaka, H.; Kobayashi, H.; Kobayashi, A.; Barzykin, V.; Gor'kov, L. P. *Phys. Rev. Lett.* **2001**, *87*, 067002.
- (18) Uji, S.; Kobayashi, H.; Brooks, J. S. *Adv. Mater. (Weinheim, Ger.)* **2002**, *14*, 243–245.
- (19) Uji, S.; Shinagawa, H.; Terashima, T.; Terakura, C.; Yakabe, T.; Terai, Y.; Tokumoto, M.; Kobayashi, A.; Tanaka, H.; Kobayashi, H. *Phys. Rev.* **2001**, *B64*, 24531.
- (20) Desiraju, G. R.; Parthasarathy, R. *J. Am. Chem. Soc.* **1989**, *111*, 8725–8726.
- (21) Legon, C. *Angew. Chem., Int. Ed.* **1999**, *38*, 2687–2714.
- (22) Ouvrard, C.; Le Questel, J.-Y.; Berthelot, M.; Laurence, C. *Acta Crystallogr.* **2003**, *B59*, 512–526.
- (23) Domercq, B.; Devic, T.; Fourmigué, M.; Auban-Senzier, P.; Canadell, E. *J. Mater. Chem.* **2001**, *11*, 1570–1575.
- (24) Imakubo, T.; Shirahata, T.; Hervé, K.; Ouahab, L. *J. Mater. Chem.* **2006**, *16*, 162–173.
- (25) Suizu, R.; Imakubo, T. *Org. Biomol. Chem.* **2003**, *1*, 3629–3631.
- (26) Imakubo, T.; Tajima, N.; Tamura, M.; Kato, R.; Nishio, Y.; Kajita, K. *J. Mater. Chem.* **2002**, *12*, 159–161.
- (27) Imakubo, T.; Sawa, H.; Kato, R. *J. Chem. Soc., Chem. Commun.* **1995**, 1097–1098.
- (28) Imakubo, T.; Sawa, H.; Kato, R. *J. Chem. Soc., Chem. Commun.* **1995**, 1667–1668.

- (29) Hervé, K.; Cador, O.; Golhen, S.; Costuas, K.; Halet, J.-F.; Shirahata, T.; Muto, T.; Imakubo, T.; Miyazaki, A.; Ouahab, L. *Chem. Mater.* **2006**, *18*, 790–797.
- (30) Ouahab, L.; Setifi, F.; Golhen, S.; Imakubo, T.; Lescouëzec, R.; Lloret, F.; Julve, M.; Ewielik, R. C. R. *Chim.* **2005**, *8*, 1286–1297.
- (31) Thoyon, D.; Okabe, K.; Imakubo, T.; Golhen, S.; Miyazaki, A.; Enoki, T.; Ouahab, L. *Mol. Cryst. Liq. Cryst.* **2002**, *376*, 25–32.
- (32) Imakubo, T.; Sawa, H.; Kato, R. *Mol. Cryst. Liq. Cryst.* **1996**, *285*, 27–32.
- (33) Nishijo, J.; Miyazaki, A.; Enoki, T.; Watanabe, R.; Kuwatani, Y.; Iyoda, M. *Inorg. Chem.* **2005**, *44*, 2493–2506.
- (34) Iyoda, M.; Kuwatani, Y.; Ogura, E.; Hara, K.; Suzuki, H.; Takano, T.; Takeda, K.; Takano, J.; Ugawa, K.; Yoshida, M.; Matsuyama, H.; Nishikawa, H.; Ikemoto, I.; Kato, T.; Yoneyama, N.; Nishijo, J.; Miyazaki, A.; Enoki, T. *Heterocycles* **2001**, *54*, 833–848.
- (35) Enoki, T.; Yamazaki, H.; Nishijo, J.; Ugawa, K.; Ogura, E.; Kuwatani, Y.; Iyoda, M.; Sushko, Y. V. *Synth. Met.* **2003**, *137*, 1173–1174.
- (36) Miyazaki, A.; Aimatsu, M.; Yamazaki, H.; Enoki, T.; Ugawa, K.; Ogura, E.; Kuwatani, Y.; Iyoda, M. *J. Phys. IV* **2004**, *114*, 545–547.
- (37) Miyazaki, A.; Aimatsu, M.; Enoki, T.; Watanabe, R.; Ogura, E.; Kuwatani, Y.; Iyoda, M. *J. Low Temp. Phys.* **2006**, *142*, 477–480.
- (38) Nishijo, J.; Miyazaki, A.; Enoki, T.; Ogura, E.; Takano, T.; Kuwatani, Y.; Iyoda, M.; Yamaura, J.-I. *Solid State Commun.* **2000**, *116*, 661–664.
- (39) Miyazaki, A.; Kato, T.; Yamazaki, H.; Enoki, T.; Ogura, E.; Kuwatani, Y.; Iyoda, M.; Yamaura, J.-I. *Phys. Rev.* **2003**, *B68*, 085108.

the π -d interactions in these conducting molecular antiferromagnets. In the present paper, we report the crystal structure, transport, and magnetic properties of two molecular conducting magnets, (EDO-TTFBr₂)₂FeCl₄ and (EDO-TTFBr₂)₂FeBr₄, and reference isomorphous salts with non-magnetic anions, (EDO-TTFBr₂)₂GaCl₄ and (EDO-TTFBr₂)₂GaBr₄, to show evidence that halogen...halogen contacts between donors and anions play essential roles in the magnetism of these conducting molecular antiferromagnets.

Experimental Section

Sample Preparations. EDO-TTFBr₂ was prepared according to the literature.³⁴ (C₄H₉)₄N⁺FeX₄ compounds (X = Cl, Br) were obtained by mixing ethanol solutions (50 mL each) of tetrabutylammonium halide (0.1 mol) and iron trihalide (0.1 mol), and then the yellow (X = Cl) or dark-red-brown (X = Br) precipitate was recrystallized from ethanol. (C₄H₉)₄N⁺GaX₄ compounds (X = Cl, Br) were synthesized by mixing aqueous solutions of gallium trihalide (obtained by dissolving 0.1 mol of gallium metal in 20 mL of concentrated hydrochloric or hydrobromic acid) and tetrabutylammonium halide (0.1 mol, 50 mL), and then the white precipitate was collected by filtration, washed with deionized water, and recrystallized from ethanol. Chlorobenzene was dried overnight with calcium hydride and distilled under argon atmosphere prior to use. Single crystalline samples of radical ion salts were obtained as thin platelike needles (typically 5 × 0.2 × 0.05 mm³) with galvanostatic ($I = 0.5 \mu\text{A}$) anodic oxidation of EDO-TTFBr₂ (4.5 mg) in an argon-purged H-shaped electrochemical cell using a Pt anode (diameter = 1 mm) and a Pt cathode (diameter = 0.5 mm) at 15 °C, with a supporting electrolyte of (C₄H₉)₄N⁺MX₄ (20 mg) in chlorobenzene (15 mL).

Crystal Structure Determination. Single crystals of the radical ion salts were mounted on a Rigaku AFC-7R four-circle diffractometer, and intensity data were collected using graphite monochromated Mo K α radiation ($\lambda = 0.71073 \text{ \AA}$). The absorption effect was empirically corrected using the ψ -scan method.⁴⁰ Structures were solved with direct methods and refined on F^2 with the full-matrix least-squares method using *SHELX 97* programs.⁴¹ For the MCl₄ salts, all non-hydrogen atoms were refined anisotropically, whereas for the MBr₄ salts only sulfur and bromine atoms were anisotropically treated due to the poor quality of the observed reflections. The positions of the hydrogen atoms were geometrically calculated and ride on the attached carbon atoms during the refinement. Crystallographic data and final reliable factors of the four salts are summarized in Table 1. Full bond lengths and bond angles, atomic coordinates, and complete crystal structure results are given as Supporting Information.

Physical Property Measurements. The electrical conductivity was measured along the stacking direction of the donor molecule (=c direction) using a dc four-probe technique between 4.2 K and room temperature. The electrical contacts were made with gold wire (20 μm diameter) and carbon paste (Dotite XC-12, Fujikura-Kasei Co., Ltd.), and measurements were performed in a constant current (~1 μA) mode. For the FeCl₄ and GaCl₄ salts, gold (~50 \AA) is deposited on the sample prior to making contacts using carbon paste, to stabilize the electrical contacts. High-pressure resistivities were measured using a Be-Cu clamp cell at up to 15 kbar with a pressure medium of Daphne-7243 oil (Idemitsu Kosan Co.). Magnetoresis-

Table 1. Crystallographic Data of the Compounds (EDO-TTFBr₂)₂MX₄

	MX ₄			
	GaCl ₄	FeCl ₄	GaBr ₄	FeBr ₄
cryst syst	ortho-rhombic	ortho-rhombic	ortho-rhombic	ortho-rhombic
space group	<i>Pnca</i> (No. 60)	<i>Pnca</i> (No. 60)	<i>Pnca</i> (No. 60)	<i>Pnca</i> (No. 60)
<i>a</i> / \AA	12.586(9)	12.587(4)	12.679(3)	12.670(4)
<i>b</i> / \AA	34.216(12)	34.246(9)	35.217(13)	35.222(7)
<i>c</i> / \AA	6.948(4)	6.952(2)	6.992(3)	6.997(4)
<i>V</i> / \AA^3	2996.6(16)	2992(3)	3122(2)	3122(2)
<i>Z</i>	4	4	4	4
measd rflns	3430	3436	1546	1085
observed rflns ($I > 2\sigma(I)$)	1371	1594	1490	1019
<i>R</i>	0.056	0.050	0.157	0.077
<i>R</i> _w	0.152	0.133	0.351	0.192

tance was measured using a 15 T superconducting magnet (Oxford Instruments) and a clamp cell at ambient and high pressures. The magnetic susceptibility was measured for aligned single crystals in the temperature range of 1.8–300 K using a Quantum Design MPMS-5 SQUID magnetometer. Samples were mounted inside a polystyrene straw with Apiezon N grease, whose contribution to the magnetization was subtracted from the observed data. Electron spin resonance (ESR) measurements were carried out with aligned single crystals, using JEOL TE-200 X-band ESR spectrometer equipped with a Oxford ESR910 helium continuous flow cryostat. Samples were mounted on a Teflon rod with Apiezon N grease and sealed in a sample tube of 5 mm diameter with 20 mmHg of helium as a heat exchange gas (1 mmHg = 133.322 Pa).

Theoretical Calculations. The energy band structures of the compounds are calculated based on the tight-binding approximation using the extended Hückel Hamiltonian.⁴² The transfer integral t between HOMOs of neighboring molecules is approximated as $t = ES$, where S is the overlap integral between HOMOs and E is the energy level of the HOMO of the EDO-TTFBr₂ donor (ca. -10 eV).

Results

Crystal Structure. Crystal structures of all four salts are isomorphous regardless of the counteranion. Parts a and b of Figure 1 present the unit cell of the FeCl₄ salt projected along the *c*- and *b*-axes, respectively. The crystal structures of these salts are close to that of (EDT-TTFBr₂)₂MBr₄ (M = Fe, Ga)³³ except the conformation of the six-membered rings of the donor molecules. The EDO-TTFBr₂ molecules lie on a crystallographic general position, and the MX₄ anions are located on a twofold axis defined by the space group symmetry (*Pnca*). The donor molecules are nearly planar except the terminal ethylenedioxy group, and there is no conformational disorder in the nonplanar six-membered rings. The MX₄⁻ anions are significantly distorted from the regular tetrahedron (minimum and maximum X-M-X angles, FeCl₄⁻, 106.41(16) and 111.87(14)°; GaCl₄⁻, 106.9(2) and 111.34(19)°; FeBr₄⁻, 104.1(3) and 112.27(15)°; GaBr₄⁻, 104.2(2) and 113.1(2)°), although no significant difference in the M-X bond lengths is observed. These anions are therefore uniaxially elongated from the regular tetrahedron along the twofold axis (|| *c*-axis).

(40) North, A. C. T.; Phillips, D. C.; Mathews, F. S. *Acta Crystallogr.* **1968**, *A24*, 351–359.

(41) Sheldrick, G. M. *SHELX97, Program for the Refinement Of Crystal Structures*; University of Göttingen: Göttingen, Germany, 1997.

(42) Mori, T.; Kobayashi, A.; Sasaki, Y.; Kobayashi, H.; Saito, G.; Inokuchi, H. *Bull. Chem. Soc. Jpn.* **1984**, *57*, 627–633.

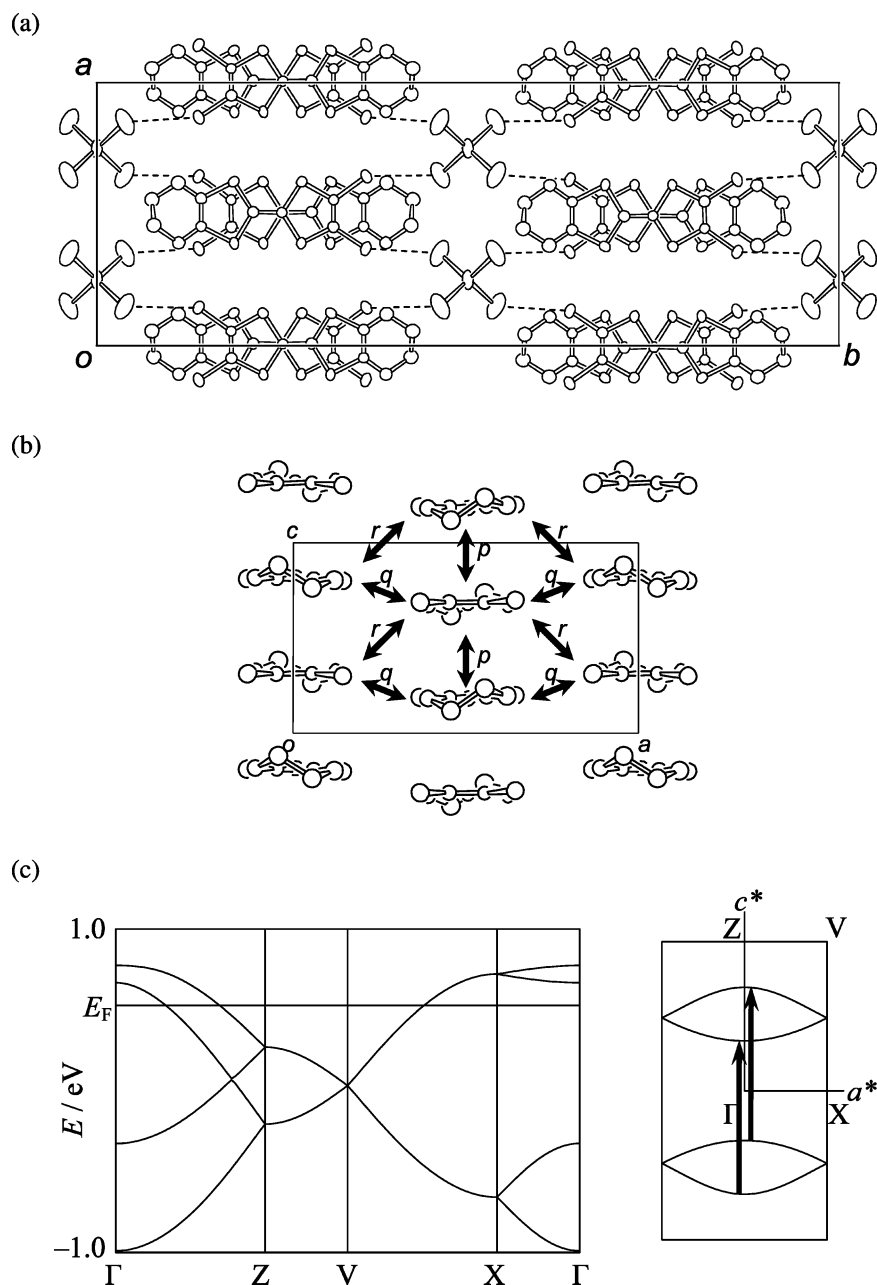


Figure 1. Crystal structure of $(\text{EDO-TTFBr}_2)_2\text{FeCl}_4$ projected along (a) the c -axis and (b) the b -axis. Dashed lines denote intermolecular $\text{Br}\cdots\text{Cl}$ contacts. Hydrogen atoms are omitted for clarity. Intermolecular overlaps p , q , and r are also indicated, whose overlap integrals are summarized in Table 2. (c) Energy dispersion curves (left) and Fermi surface (right) calculated based on the tight-binding approximation using the extended Hückel Hamiltonian. The solid arrows represent a nesting vector of the quasi-1D Fermi surfaces.

The donor molecules are stacked to form one-dimensional columns along the c -axis as illustrated in Figure 1b, and the anions are sandwiched between these donor columns. The neighboring two donor molecules inside a column are related by the c -glide plane ($\perp b$ -axis) symmetry; hence, the donor molecules are uniformly aligned in the columns. A number of intermolecular $\text{S}\cdots\text{S}$ contacts are observed both within and between columns, with distances slightly longer than the vdW distance between sulfur atoms (3.60 Å).⁴³ It should also be mentioned that close $\text{Br}\cdots\text{S}$ contacts are present between the neighboring columns, whose distances (FeCl_4 , 3.612(2) Å; GaCl_4 , 3.620(3) Å; FeBr_4 , 3.589(6) Å; GaBr_4 ,

3.636(9) Å) are significantly shorter than the $\text{Br}\cdots\text{S}$ vdW distance (3.65 Å).⁴³ For the anion layers, intermolecular halogen–halogen contacts are weak for MBr_4 salts and negligible for MCl_4 salts, judging from the comparison of the halogen–halogen distances (FeBr_4 , 3.848(6) Å; GaBr_4 , 3.905(10) Å; FeCl_4 , 3.949(5) Å; GaCl_4 , 3.955(7) Å) with the corresponding vdW distances ($\text{Br}\cdots\text{Cl}$, 3.60 Å; $\text{Br}\cdots\text{Br}$, 3.70 Å).⁴³ The most remarkable intermolecular contacts in these salts are short $\text{Br}\cdots\text{X}$ contacts observed between the bromide substituent of the donors and the halide ligand of the anions, whose distances (FeCl_4 , 3.348(4) Å; GaCl_4 , 3.357(5) Å; FeBr_4 , 3.432(5) Å; GaBr_4 , 3.507(7) Å) are significantly shorter than the corresponding vdW distances. Due to these

(43) Bondi, A. *J. Phys. Chem.* **1964**, *68*, 441–451.

Table 2. Calculated Intermolecular Overlap Integrals ($\times 10^3$) of the Compounds (EDO-TTFBr₂)₂MX₄^a

integral	MX ₄			
	GaCl ₄	FeCl ₄	GaBr ₄	FeBr ₄
<i>p</i>	-37.1	-36.5	-34.9	-35.5
<i>q</i>	-6.48	-6.56	-6.33	-7.19
<i>r</i>	-11.08	-10.98	-11.80	-9.93

^a See Figure 1c for the definitions of the intermolecular overlaps.

contacts, the anions in these compounds are linked to the nearest-neighboring donor molecules rather than making an anion network. The origin of the uniaxial distortion of the MX₄⁻ anion is also explained by the presence of these short intermolecular halogen–halogen contacts.

Band Structure Calculations. Since these four compounds are isomorphous, each salt gives a similar energy band structure. Table 2 summarizes the intermolecular overlap integrals between the HOMOs of the neighboring donor molecules, in which the definitions of the overlapping modes between the donors are shown in Figure 1b. The absolute values of the overlap integrals along the stacking direction (*p*) are 3–5 times larger than those along the side-by-side direction (*q*, *r*), suggesting a quasi-1D electronic nature of the π -electron system. Comparison between the four MX₄ (M = Fe, Ga) salts reveals that the MCl₄ salts have a tendency of giving a larger *p* and smaller *q*, *r* than the MBr₄ salts; hence, the quasi-1D nature of the former salts is more prominent than that of the latter salts. Figure 1c shows the dispersion curves and the Fermi surfaces of the FeCl₄ salt. There are four dispersion curves with larger dispersion in the Γ -X direction than the Γ -Z direction, and the lentil-like Fermi surface is explained as parallel warped lines perpendicular to the *c*-axis, which is folded along the Γ -X direction due to the space group symmetry. Thus, the electronic nature of the present system can be characterized as a quasi-1D metallic system having open-orbit Fermi surfaces, which possess the nesting vector as illustrated with the thick arrows in Figure 1c.

Electrical Conductivities. Parts a–d of Figure 2 present the temperature dependence of the resistivities ρ for the GaCl₄, FeCl₄, GaBr₄, and FeBr₄ salts, respectively, measured along the donor stack direction ($\parallel c$) at various pressures. All plots are normalized with the resistivity at room temperature. At ambient pressure, although the metallic behavior was observed around the room temperature for all of these salts, no reproducible results are obtained due to the generation of cracks caused by the thermal contraction of the samples and, thus, these are omitted from the plots. Under pressure, all these salts show considerable low room-temperature resistivities ($\sim 10^{-2} \Omega \text{ cm}$) that monotonically decrease as the pressure increases. As the temperature decreases, the resistivity shows metallic behavior in the high-temperature region regardless of the counteranion, and it increases in the low-temperature region after taking a minimum. As shown in the figures, the temperatures for this resistivity minimum monotonically decrease for each compound as the pressure increases. On comparison of the resistivities of the MCl₄ and MBr₄ salts, the latter have the

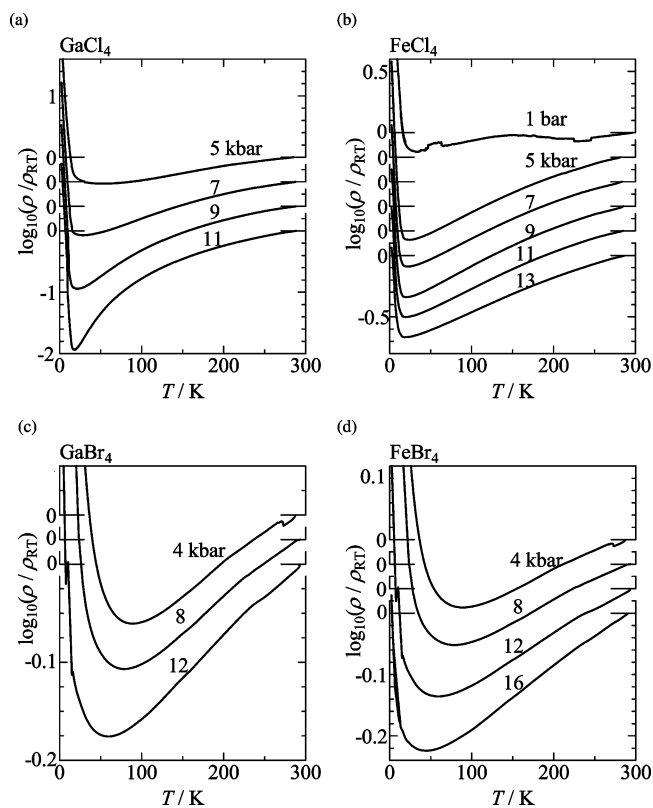


Figure 2. Temperature dependence of the resistivity of the (a) GaCl₄, (b) FeCl₄, (c) GaBr₄, and (d) FeBr₄ salts under various pressures, normalized with the value at room temperature.

higher resistivity minimum temperature. However, this does not mean that the MBr₄ salts have a higher metal–insulator transition temperature than MCl₄ salts, as evidenced from the ESR results discussed later. Parts a and b of Figure 3 show the temperature dependence of $d(\ln(\rho))/d(T^{-1})$ under pressure for the GaCl₄ and FeCl₄ salts, respectively. For the GaCl₄ salt, two peaks of P1 and P2 are observed around 16 and 13 K at 5 kbar, respectively, and their peak temperatures decrease as the pressure increases. For the FeCl₄ salt, another peak A, corresponding to the kinks in the ρ vs *T* plot, appears around 5 K at 5 kbar, and the temperature of this additional peak increases and its shape becomes more prominent as the pressure increases.

Magnetic Susceptibilities. The magnetic susceptibility of the GaCl₄ salt gives a nearly temperature-independent value of $4.5 \times 10^{-4} \text{ emu mol}^{-1}$ from 2 to 300 K after the subtraction of the Curie contribution in the low-temperature region that can be attributed to impurities. This result is explained as a Pauli paramagnetism derived from the metallic nature of this salt. Due to the small amount of the obtained GaBr₄ salt, no reliable susceptibility data are obtained. Parts a and c of Figure 4 present the magnetic susceptibilities of the FeCl₄ and FeBr₄ salts, respectively, measured along the three crystallographic axes under the external field of 1 T. Parts b and d of Figure 4 are the magnetization curves of the FeCl₄ and FeBr₄ salts, respectively, measured at 2 K. In the high-temperature region (FeCl₄ > 50 K, FeBr₄ > 150 K), the susceptibilities of both salts obey the Curie–Weiss law. The Curie constants (FeCl₄, $4.8 \text{ emu K}^{-1} \text{ mol}^{-1}$; FeBr₄, $4.4 \text{ emu K}^{-1} \text{ mol}^{-1}$) show that susceptibility is governed by the

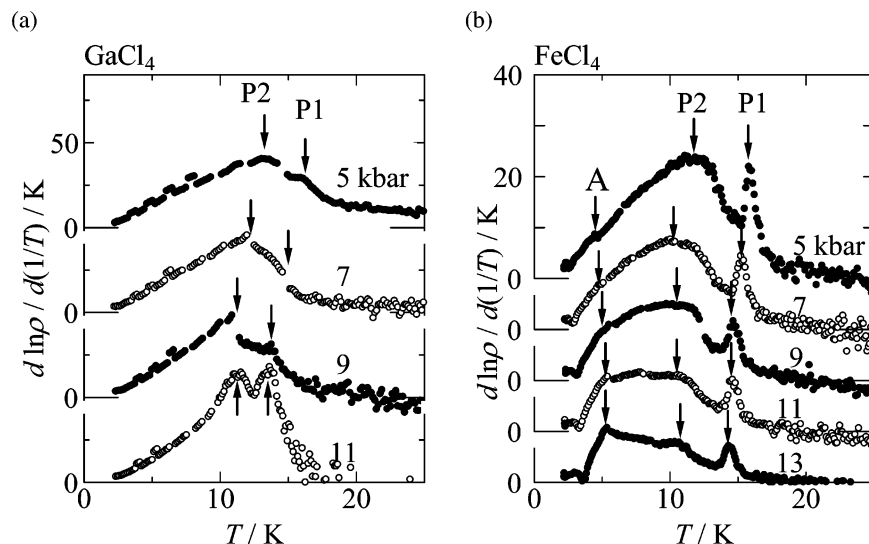


Figure 3. Temperature dependence of $d(\ln(\rho))/d(1/T)$ of the (a) GaCl_4 and (b) FeCl_4 salts under pressures. Arrows with P1, P2, and A indicate anomalies described in the text.

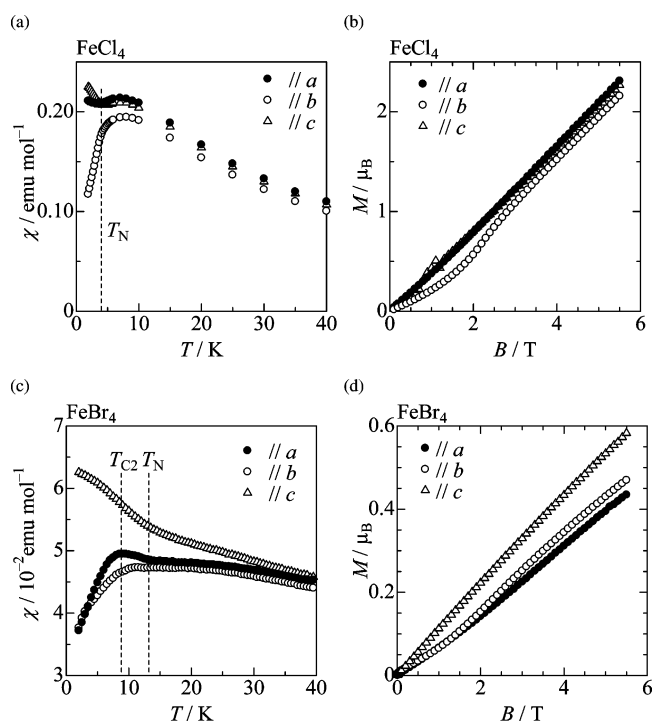


Figure 4. (a) Temperature dependence of the static magnetic susceptibility of the FeCl_4 salt measured with the external field $B = 1$ T, after the core diamagnetic contribution is subtracted. (b) The magnetization curve measured at $T = 2$ K. (c) Temperature dependence of the static magnetic susceptibility of the FeBr_4 salt measured with the external field $B = 1$ T, after the core diamagnetic contribution is subtracted. (d) The magnetization curve measured at $T = 2$ K. The field is applied along the a - (filled circles), b - (open circles), and c -axes (open triangles).

high spin ($S = 5/2$) state of the FeX_4^- anions, and the Weiss temperatures (FeCl_4 , -9.0 K; FeBr_4 , -23 K) show the presence of the antiferromagnetic interaction between the d-electron spins. In a low-temperature region ($\text{FeCl}_4 < 50$ K, $\text{FeBr}_4 < 150$ K), the susceptibility significantly deviates from the Curie–Weiss behavior. The susceptibility of the FeCl_4 salt shows a broad peak of short-range order around 7 K, and then an antiferromagnetic transition takes place at $T_N = 4.2$ K. From the anisotropy of the susceptibility below

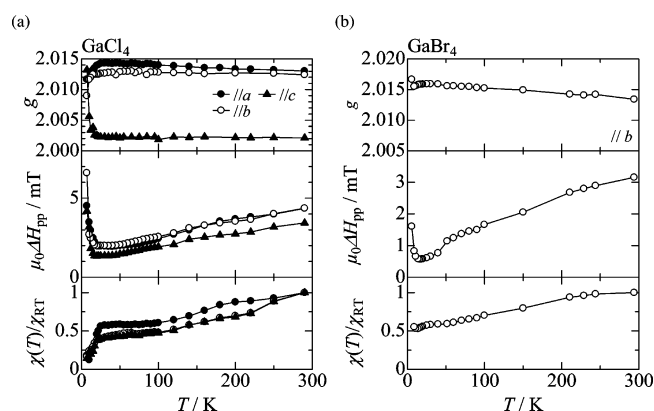


Figure 5. Temperature dependence of the g -value (top panel), the peak-to-peak line width $\mu_0\Delta H_{pp}$ (middle panel), and the spin susceptibility (bottom panel), normalized by the value at 290 K of the (a) GaCl_4 and (b) GaBr_4 salts. The field is applied along the a - (filled circles), b - (open circles), and c -axes (filled triangles). Solid lines are guides for eyes.

T_N and the presence of the spin–flop transition (Figure 4b, $B_{ST} = 2$ T at $T = 2$ K), the spin-easy axis is assigned to the b -axis. For the FeBr_4 salt, the susceptibility along the c -axis deviates from the other two axes below ca. 30 K, then at $T_N = 13.5$ K an AF transition takes place, below which point the susceptibility increases along the a - and c -axes and decrease along the b -axis are observed, showing the spin-easy axis parallel to the b -axis. At $T_{C2} = 8.5$ K, another anomaly is observed, where the susceptibility along the a -axis shows a maximum and begins to decrease below this temperature. On the magnetization curves measured at 2 K, a spin–flop transition is observed at $B = 1.8$ T for both $B \parallel a$ and $B \parallel b$ directions (Figure 4d). This suggests the presence of noncollinear spin structure without a unique spin-easy axis in the magnetically ordered state. From the magnetization curves, the saturation fields for the FeCl_4 and FeBr_4 salts are estimated at 12 and 45 T, respectively, as the fields where extrapolated magnetization curves reach $5 \mu_B$.

Electron Spin Resonance. Parts b of Figure 5 present the temperature dependencies of the ESR g -values (upper panel), the peak-to-peak line widths $\mu_0\Delta H_{pp}$ (middle panel,

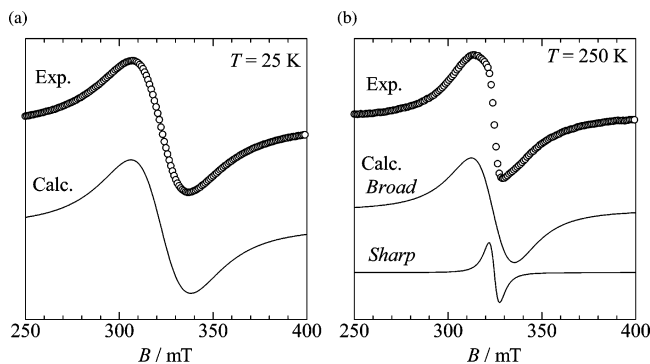


Figure 6. ESR spectra of the FeCl_4 salt ($\parallel b$ -axis) at (a) $T = 25$ K and (b) $T = 250$ K. In the figures the open circles are experimental data and the solid lines are Lorentzian line shapes obtained by the least-squares fittings. For $T = 250$ K, two Lorentzian curves of “broad” and “sharp” are necessary to reproduce the experimental data.

$\mu_0 = 4\pi \times 10^{-7} \text{ T}^2 \text{ J}^{-1} \text{ m}^3$ is the vacuum permeability), and the spin susceptibilities (lower panel, normalized at the value of 290 K) for the GaCl_4 and GaBr_4 salts, respectively. The ESR spectra of GaX_4 salts with diamagnetic anions are well fitted with a single Lorentzian line-shape function in the whole temperature range. The g -values along the three crystallographic axes are characteristic of the TTF cation radical.⁴⁴ For the GaCl_4 salt, the g -value slightly increases ($\parallel a$) or becomes almost temperature independent ($\parallel b, c$) as the temperature decreases to ca. 25 K, below which point significant downward ($\parallel a, b$) and upward ($\parallel c$) shifts are observed. Both the line width and spin susceptibility decrease as the temperature decreases to ca. 20 K. Below this temperature the line width increases and diverges at 7 K. The spin susceptibility rapidly decreases below this temperature regardless of the direction of the static magnetic field. The ESR signal of the GaBr_4 salt shows the temperature dependence of the g -value, the line width, and the spin susceptibility that are similar to the GaCl_4 salt in the higher temperature region and the small g -value shift and increase in the line width that are observed at ca. 15 K.

The ESR spectra of the FeCl_4 and FeBr_4 salts are well fitted with single Lorentzian signals (Figure 6a, $T = 25$ K) below $T = 30$ and 40 K, respectively, and are expressed as sums of sharp and broad Lorentzian signals above these temperatures, as illustrated in Figure 6b ($T = 250$ K). Parts a and b of Figure 7 present the temperature dependencies of the g -values, the line widths, and the spin susceptibilities of the sharp and broad signals for the FeCl_4 salt, respectively, and parts c and d of Figure 7 show the same plots for the FeBr_4 salts. The g -values along the three crystallographic axes for the sharp signals of both salts are characteristic of the TTF cation radical, and the spin susceptibilities of the broad signals are more than 10 times greater than those of the sharp signals. Therefore, the sharp signals are attributed to the π -electron spins, and the broad signals come from the d-electron spins. For the FeCl_4 salts, the g -values of both sharp and broad signals have little temperature dependence for $B \parallel a, b$, whereas the g -value for $B \parallel c$ decreases as the

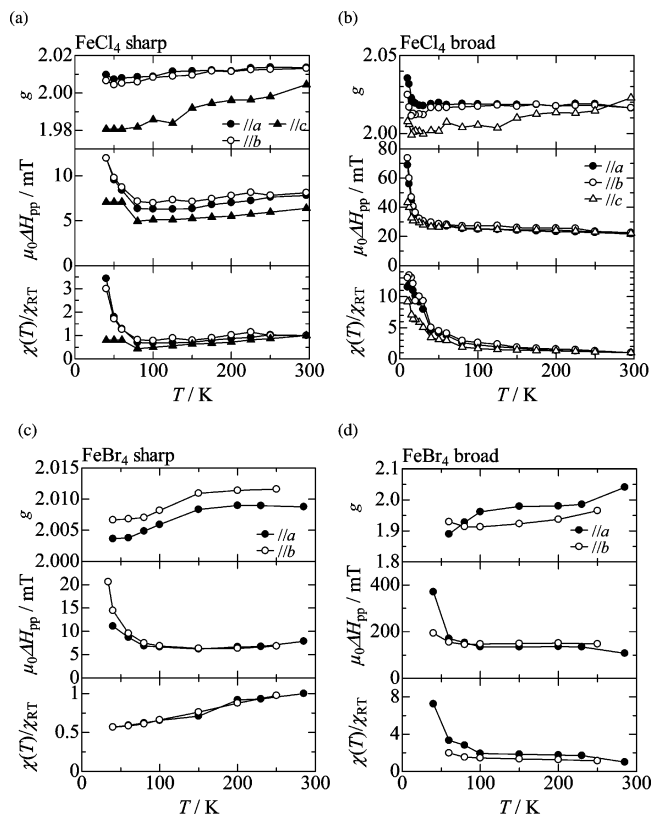


Figure 7. Temperature dependence of the g -value (top panel), the peak-to-peak line width $\mu_0\Delta H_{pp}$ (middle panel), and the spin susceptibility (bottom panel), normalized by the value at 290 K for the (a) sharp and (b) broad signal of the FeCl_4 salt and the (c) sharp and (d) broad signal of the FeBr_4 salt. The field is applied along the a - (filled circles), b - (open circles), and c -axes (open triangles). Solid lines are guides for eyes.

temperature decreases. At around $T = 30$ K, the sharp and broad signals coalesce into a single Lorentzian signal, and at around $T = 20$ K, the g -values show upward shifts in all directions. The line width of the sharp signal slightly decreases as the temperature decreases above 80 K and then increases in the vicinity of the coalescence temperature. For the broad signals, the line width monotonically increases as the temperature decreases. Below ca. 20 K, the line width of the signal after coalescence increases rapidly and diverges at 7 K. The spin susceptibility of the sharp signal slightly decreases as the temperature decreases to the vicinity of the coalescence. The spin susceptibility of the broad signal increases as the temperature decreases, which corresponds to the Curie–Weiss behavior of the static susceptibility of the magnetic anion. For the FeBr_4 salts, both sharp and broad signals are observed only above ca. 40 K, due to the coalescence of these signals into a single signal which is too broad to be observed. The g -values of the sharp signal slightly decrease as the temperature decreases in the range of 100–150 K. The g -value of the broad signal also shows a decreasing trend, although these values have low accuracy due to the large line width of the peaks (> 100 mT). The line width of the sharp signals gradually decreases as the temperature decreases and begins to increase below 100 K and diverges below 40 K. The line width of the broad signals is nearly temperature independent above ca. 80 K, below which point it begins to diverge. The spin susceptibility of

(44) Sugano, T.; Saito, G.; Kinoshita, M. *Phys. Rev.* **1987**, *B35*, 6554–6559.

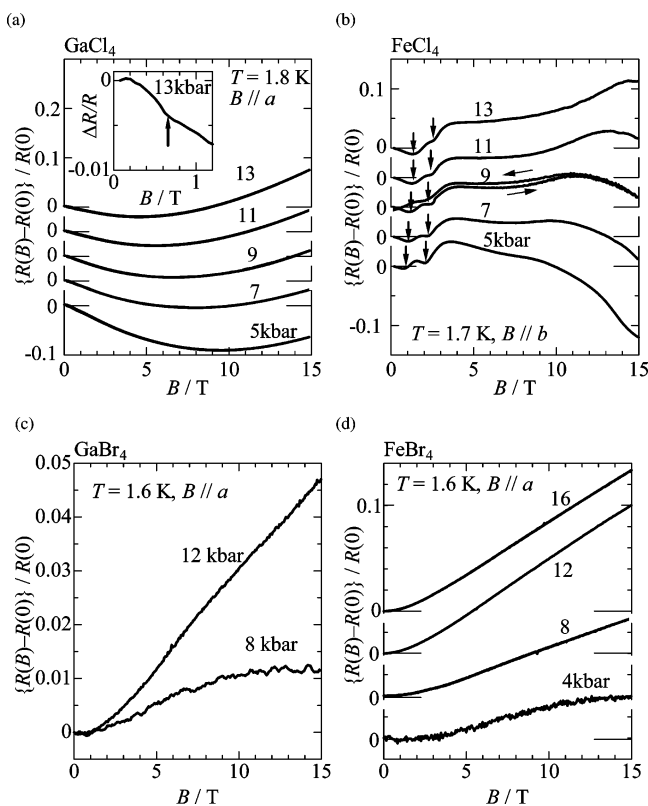


Figure 8. Magnetoresistance of the (a) GaCl₄, (b) FeCl₄, (c) GaBr₄, and (d) FeBr₄ salts under various pressures. The inset of (a) is an expanded view of the magnetoresistance of the GaCl₄ salt at $p = 13$ kbar, where an anomaly is observed at around $B = 0.6$ T (indicated with an arrow). For the FeCl₄ salt (b), stepwise anomalies are indicated with arrows, and the hysteresis is also shown for $p = 9$ kbar.

the sharp signal gradually decreases as temperature decreases, and at 40 K it reaches half the value of that of room temperature. As for the broad signal, the spin susceptibility increases as the temperature decreases, corresponding to the Curie–Weiss behavior of the static susceptibility of the magnetic anion.

Magnetoresistance. Parts a–d of Figure 8 show the magnetoresistance (MR) of the GaCl₄, FeCl₄, GaBr₄, and FeBr₄ salts, respectively, under various pressures. In the low-field region, the GaCl₄ salt shows negative MR and a quadratic field dependence is observed at higher fields (Figure 8a). As the pressure increases, the magnetic field of the MR minimum B_{\min} decreases monotonically (10 T at 3 kbar, 5 T at 3 kbar), and the magnitude of the negative MR at B_{\min} also decreases (-10.5% at 3 kbar, -2.0% at 13 kbar). As a result, the MR at 15 T increases from -8.5% at 3 kbar to $+7.3\%$ at 13 kbar. In addition, a very small anomaly is observed at $B = 0.7$ T in the MR vs magnetic field curve when the field is applied along the a -axis, as shown in the inset of Figure 8a for $p = 13$ kbar data, for example. This anomaly is observed in the whole pressure range, without distinct pressure dependence.

Compared with the GaCl₄ salt, the MR of the FeCl₄ salt shows more complicated behaviors, especially when the field is applied along the b -axis (Figure 8b). Around zero magnetic field, the MR decreases as the field increases. Then there are two stepwise increases in MR around 1 and 2 T, which

are indicated in Figure 8b with arrows. As the pressure increases, the fields for these anomalies monotonically increase. In the intermediate field region (ca. 4–10 T), the MR has a large pressure dependence. For the MR at 5 kbar a decreasing trend is observed, whereas at 7 kbar the MR is nearly field independent, and above 9 kbar the MR increases as the magnetic field increases. In the high-field region (> 10 T), the MR begins to decrease as the field increases. At $p = 5$ kbar, the negative slope of the MR curve becomes prominent above $B = 12$ T. Above 9 kbar, a MR maximum is observed, whose magnetic field increases as the pressure increases (11 T at 9 kbar, 14 T at 13 kbar). It must also be noted that the MR curve shows a hysteresis below ca. 10 T (shown only for 9 kbar in Figure 8b for simplicity of the figure). Namely, the MR in the demagnetization process has a larger value than in the magnetization process. For the two MBr₄ salts, small positive magnetoresistance is observed ($+5$ and $+14\%$ for the GaBr₄ and FeBr₄ salts, respectively), showing quadratic field dependence below ca. 3 T and linear field dependence above this field in pressures above 12 kbar for both salts.

Discussion

Ground State of the π -Electron System. We first discuss the nature of the π -electron system of these salts based on the results for the GaCl₄ salt. Due to the similarity in the crystal structure of all four salts, we can assume that these salts have similar ground states in the π -electron side. We adopt the GaCl₄ salt as representative, since, compared to the other salts, the detailed behavior of the GaCl₄ salt observed in the experiments is well qualified for further analysis.

The GaCl₄ salt exhibits metallic behavior around room temperature, as evidenced by the conductivity under pressure above 5 kbar and the susceptibility at ambient pressure. The spin susceptibilities measured by ESR and SQUID can be assigned as Pauli paramagnetic susceptibility and show a gradual decrease as the temperature decreases. This temperature dependence can be explained to result from thermal contraction of the donor columns and/or partial localization of the conduction π -electrons due to the electron correlation. In the first explanation, the tight-binding band structure model shows that the Pauli susceptibility of a 1D metallic system is roughly proportional to $1/t_{\parallel}$ where the transfer integral t_{\parallel} along the conduction column increases as a result of the thermal contraction as the temperature decreases. The partial charge localization gives the susceptibility that obeys the 1D Heisenberg antiferromagnet model having an exchange interaction whose magnitude exceeds the thermal energy at room temperature;⁴⁵ thus, the small positive gradient in the susceptibility vs temperature plot is expected, as observed in the experiment.

The temperature dependence of the ESR line width also supports the metallic behavior of this salt. In quasi-1D conductors the spin–lattice relaxation process is governed

(45) Dumm, M.; Loidl, A.; Fravel, B. W.; Starkey, K. P.; Montgomery, L. K.; Dressel, M. *Phys. Rev.* **2000**, *B61*, 511–521.

by the Elliott mechanism,⁴⁶ and the ESR line width is expressed as $\mu_0\Delta H_{pp} \propto 1/T_1 \propto (\Delta g)^2/\tau$, where T_1 is the spin-lattice relaxation time, $\Delta g \equiv g - 2.0023$ is the g -value shift from the free-electron value, and τ is the relaxation time of the conduction electrons. As the resistivity ρ is given as $\rho = m^*/(ne^2\tau)$ where m^* is the effective mass of the conduction electrons and n is the carrier density, the line width $\mu_0\Delta H_{pp}$ is proportional to the resistivity ρ , which is evidenced by the similar temperature dependence of $\mu_0\Delta H_{pp}$ at ambient pressure (Figure 5a) and ρ under pressure (Figure 2a).

In the low-temperature region, the metallic behavior of this salt gradually turned into a semiconducting behavior. One possible origin of the semiconducting ground state is the instability of quasi-1D electronic nature, as suggested by the band structure calculations where the presence of a nesting vector (arrows in Figure 1c) is preferable for the electronic instability. The ESR spectra show that the spin-density wave (SDW) state is the most plausible candidate for the ground state of this salt. The steep decrease of the spin susceptibility below 25 K (Figure 5a) evidences the disappearance of the conduction electrons, and the divergence of the line width below 10 K indicates the development of the internal magnetic field in the magnetically ordered SDW state. In addition, the anisotropic shift in the g -value is the consequence of the growth of short-range order of the localized spins in low-dimensional magnetic systems.⁴⁷

The presence of the SDW transition is evidenced also in the transport properties under pressure. The temperature dependence of $d(\ln(\rho))/d(T^{-1})$ for the GaCl₄ salt (Figure 3a) shows two peaks P1 and P2 at temperatures of T_{P1} and T_{P2} , respectively. As T_{P1} is close to the temperature of the ESR anomaly, the peak P1 corresponds to the SDW transition of the π -electron system. The presence of another peak P2 is suggestive of the feature of successive transitions in the electronic stabilization to the SDW state, although their detailed mechanism is not clear yet. As the pressure increases, both T_{P1} and T_{P2} decrease, showing the stabilization of the metallic state caused by the application of the pressure. This is caused by the increase of the transfer integrals, along both the stacking direction and the side-by-side direction.

The behavior of the longitudinal magnetoresistance (MR, Figure 8a) also supports the presence of the SDW state in the GaCl₄ salt. At a first glance, the field dependence of the SDW transition is opposite to that of the TMTSF salts, in which the transition temperature T_{SDW} increases nearly quadratically with the field in low magnetic fields.⁴⁸ This behavior is explained by the mean-field theory, based on the nesting of the slightly warped, quasi-1D Fermi surfaces.⁴⁹ On application of the field, the total energy of the SDW is lowered by the quantization of the closed orbits near the Fermi level, i.e., recovery of the one-dimensional character of electron band in the magnetic field. On the other hand, in the present compounds the low-dimensional character is

weaker and less sensitive to the external field than that of the Bechgaard salts. Therefore, this system shows a field dependence of the transition temperature typical to that of the magnetically ordered system, and the presence of the negative MR can be explained as a competition between the field-induced reduction in the gap and the emergence of the orbital MR contribution. Assuming that the gap energy has the phenomenological BCS-like field dependence

$$E_{SDW}(B) = E_{SDW}(0)[1 - (B/B_c)^2] \quad (1)$$

where B_c is a critical field, the resistivity under the magnetic field is expressed as

$$\rho(B) = \rho(0) \exp\left[\frac{E_{SDW}(0)\{1 - (B/B_c)^2\}}{k_B T}\right] \quad (2)$$

The MR is a sum of the negative contribution of the disappearance of the SDW state as expressed in eq 2 and the positive contribution of the Lorentz force that works on the conduction electrons. Since the present salt has the quasi-1D open-orbit Fermi surface as shown in the band structure calculation, the latter contribution is proportional to B^2 in the high-field limit.⁵⁰ The field dependence of MR is therefore expressed as

$$\Delta\rho(B)/\rho(0) = \alpha\left(\exp\left[\frac{E_{SDW}(0)\{1 - (B/B_c)^2\}}{k_B T}\right] - 1\right) + \gamma B^2 \quad (3)$$

where α is a field-independent coefficient of the negative MR contribution and the factor γ corresponds to the square of the carrier mobility $\mu = e\tau/m^*$. The fitting of eq 3 to the experimental result is satisfactory as illustrated in Figure 9a. Figure 9b summarizes the pressure dependence of the SDW gap at zero field $E_{SDW}(0)$ and the parameter γ . As the pressure increases, $E_{SDW}(0)$ decreases and γ increases monotonically. The increase in γ means an increase in the carrier mobility μ occurs, which can be understood as an increase of the scattering time τ and/or a decrease of the effective mass m^* . From the structural viewpoint, the latter is related to the increase of the transfer integrals by applying the pressure, which leads to larger curvature of the dispersion curves in the band structure model.

Finally, we compare the results of the GaBr₄ salt with those of the GaCl₄ salt to elucidate effects of the counterion. In the ESR spectra of the GaBr₄ salt (Figure 5b), the divergence of the line width appears only symptomatically at the lowest temperature. Since the GaBr₄ and GaCl₄ salts are isomorphous, it is reasonable to assume for the following reason that the ground state of the GaBr₄ salt is also an SDW state having a lower transition temperature. Comparison of the transfer integrals of these two salts reveals that the GaBr₄ salt has larger side-by-side transfer integrals than the GaCl₄ salt. This suggests that the quasi-1D nature of the π -electron system of the GaBr₄ salt is suppressed compared with the

(46) Elliot, R. J. *Phys. Rev.* **1954**, *96*, 266–279.

(47) Nagata, K.; Tazuke, Y. *J. Phys. Soc. Jpn.* **1972**, *32*, 337–345.

(48) Matsunaga, N.; Yamashita, K.; Kotani, H.; Nomura, K.; Sasaki, T.; Hanajiri, T.; Yamada, J.; Nakatsuji, S.; Anzai, H. *Phys. Rev. B* **2001**, *64*, 052405.

(49) Montambaux, G. *Phys. Rev. B* **1988**, *38*, 4788–4795.

(50) Singleton, J. *Band Theory and Electronic Properties of Solids*; Oxford University Press, 2001.

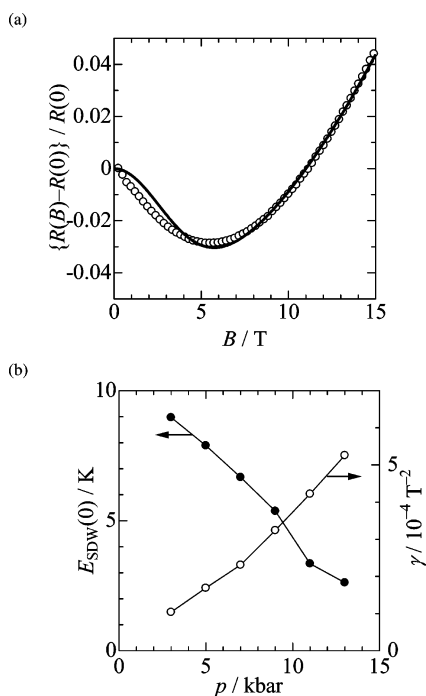


Figure 9. (a) Fitting of the magnetoresistance (solid line, see text) to the experimental data (open circles) at $p = 11$ kbar. (b) Pressure dependence of the SDW band gap $E_{\text{SDW}}(0)$ and parameter γ that corresponds to the square of the carrier mobility (see text). Solid lines are guides for the eyes.

GaCl₄ salt and gives the lower SDW transition temperature. In fact, MR of the GaBr₄ salt measured at $T = 1.7$ K (Figure 8c) shows no negative contribution that should appear in the SDW state as in the case of the GaCl₄ salt (Figure 8a), suggesting that the real SDW transition temperature of the GaBr₄ salt lies below this temperature. The higher minimum temperature of the GaBr₄ salt (Figure 2c) compared with that of the GaCl₄ salt (Figure 2a) does not contradict the lower SDW transition temperature of the GaBr₄ salt, since this resistivity minimum is due to a gradual change from the metallic to the insulating phase and the minimum temperature does not coincide with the real metal-to-insulator phase transition temperature. In fact, even for the GaCl₄ salt, the resistivity minimum temperature (~ 50 K at 5 kbar) is slightly higher than the SDW transition temperature ($T_{\text{P1}} = 16$ K at 5 kbar).

Magnetic Structure of the d-Electron System. Next, we discuss the magnetic properties of the FeCl₄ and FeBr₄ salts having the magnetic counteranions, mainly focused on the behaviors of the d-electron spins. The negative Weiss temperature (FeCl₄, -9.0 K; FeBr₄, -23 K) shows the presence of the antiferromagnetic exchange interaction between the d-electron spins. Between the magnetic ions in the FeCl₄ salt, however, no significant Cl \cdots Cl contacts are observed, which otherwise play a major role in exchange interaction. The only possible counterpart of the intermolecular contacts for a FeCl₄⁻ anion is the bromide substituent of the donor molecule; hence, the π -electron system of the donor layer must mediate the antiferromagnetic exchange interaction between the FeCl₄⁻ anions. For the FeBr₄ salt, on the other side, FeBr₄⁻ anions are connected to form zigzag chains with intermolecular Fe–Br \cdots Br–Fe contacts. How-

ever, due to their distances ($3.871(8)$ Å) being significantly longer than the vdW distance (3.70 Å),⁴³ these contacts are not close enough to explain the large antiferromagnetic interaction between the FeBr₄⁻ anions, which is suggested by the large saturation field (45 T) estimated from the extrapolation of the magnetization curves. It is therefore suggested that the participation of the donor π -electron system reinforces the antiferromagnetic interaction between the magnetic anions.

The magnetism of the FeCl₄ salt can be described as a simple collinear low-dimensional antiferromagnet. The susceptibility takes a broad peak around 7 K, which implies the presence of the magnetic short-range ordering (Figure 4a). In the antiferromagnetic phase below $T_{\text{N}} = 4.2$ K, the spin-easy axis is parallel to the b -axis, which is evidenced from the magnetization curves (Figure 4b). This easy-axis direction coincides with the direction where the dipole–dipole interaction energy takes a minimum ($\parallel a$, $+0.44$ K; $\parallel b$, -0.56 K; $\parallel c$, $+0.11$ K),⁵¹ showing that the orientation of the easy axis is determined from the dipole–dipole interaction between the FeCl₄⁻ anions. Below T_{N} , the susceptibility along the c -axis shows an increase with quadratic behavior as the temperature decreases, which can be explained from the spin-wave theory.^{52–54} The increase of the perpendicular susceptibility χ_{\perp} from the molecular field value is more prominent for lower lattice dimensions and/or smaller spin quantum numbers. The magnetism of the present FeCl₄ salt can be therefore characterized as a quasi-1D chain through anion \cdots donor \cdots anion contacts.

On the other hand, the magnetic properties of the FeBr₄ salt show complicated behaviors. Compared with the a - and b -directions, the susceptibility along the c -axis is significantly larger below 30 K (Figure 4c). This direction corresponds to the uniaxial strain of the tetrahedral counteranions. In a crystal field of T_d symmetry, the d-electrons of a high-spin Fe³⁺ ion (d^5) are in the isotropic 6A_1 ($t_2^3e^2$) configuration. However, if the contributions from the 4T_1 ($t_2^2e^3$) excited states and the metal–ligand covalent character are taken into account, a single-ion anisotropy due to the spin–orbit coupling appears as a function of the distortion from the T_d symmetry, which is both theoretically and experimentally evidenced for Ph₄P \cdot FeCl₄.⁵⁵ Namely, uniaxially compressed FeCl₄⁻ anion in this salt gives a negative single-ion anisotropy parameter $D < 0$. In the present case, the FeBr₄ anion is uniaxially *elongated* as a result of close TTF–Br \cdots Br–Fe contacts between the donors and anions; hence, this anion should have a positive single-ion anisotropy parameter $D > 0$. The anion spins therefore prefer to lie on the ab -plane rather than in the c -direction; hence, the magnetic susceptibility along the a - and b -direction is smaller than that along the c -axis. This magnetic anisotropy is not significant for

(51) In the calculation the spins are treated as a point dipole vector located on the iron atoms, assuming an antiparallel spin alignment. The sum of the dipole–dipole interaction energy between spin pairs was taken within the radius of 50 Å.

(52) Oguchi, T. *Phys. Rev.* **1960**, *117*, 117–123.

(53) Kubo, R. *Phys. Rev.* **1952**, *87*, 568–580.

(54) Anderson, P. W. *Phys. Rev.* **1951**, *83*, 1260–1260.

(55) Deaton, J. C.; Gebhard, M. S.; Solomon, E. I. *Inorg. Chem.* **1989**, *28*, 877–889.

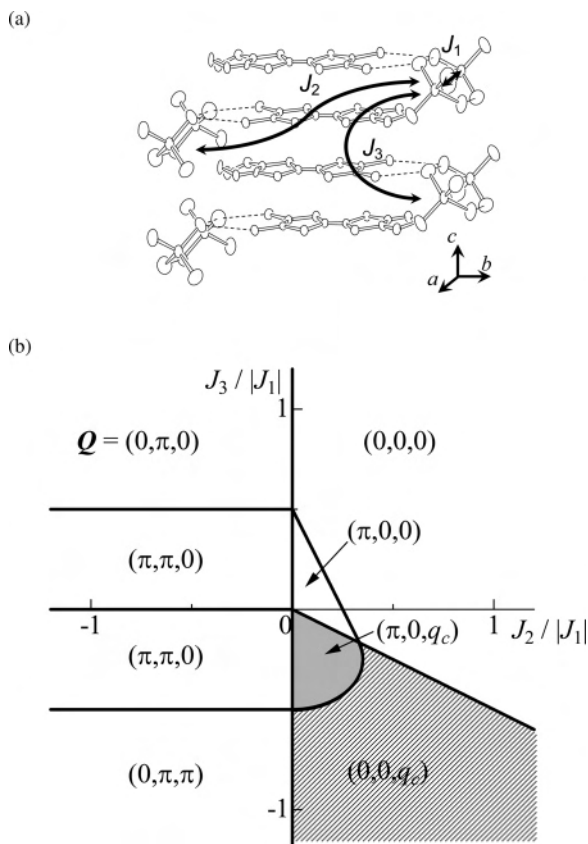


Figure 10. (a) Three intermolecular exchange interaction paths between the anions in the FeBr_4 salt. (b) Phase diagram of the ground state spin structure as a function of the normalized exchange interaction $J_2/|J_1|$ and $J_3/|J_1|$. In each region the wavevector $\mathbf{Q} = (q_a, q_b, q_c)$ that maximizes the Fourier component of the exchange interaction J is presented. The shaded and hatched regions are possible helical spin structures of the FeBr_4 salt with $q_c = 2 \cos^{-1}(|J_2/2J_3|)$.

the FeCl_4 salt, although the anion tetrahedron is similarly distorted, which can be explained from the smaller spin-orbit interaction for the Cl ligand than for the Br ligand.

At $T_N = 13.5$ K, an antiferromagnetic transition takes place with the spin-easy axis parallel to the b -axis (Figure 4c). The temperature dependence of the susceptibility below T_N is different from that of the typical antiferromagnet, in the point that the susceptibility increases as the temperature decreases for both a - and c -axes. At $T_{C2} = 8.5$ K, the susceptibility along the a -axis shows a maximum and begins to decrease as the temperature decreases. As the temperature T reaches 0 K, the susceptibilities along the a - and b -axes decrease and approach finite positive values, and in the magnetization curves (Figure 4d) the spin-flop transitions are observed around 1.8 T for both of these directions. These behaviors of the magnetic anisotropy are characteristic of the helical-ordered spin state.

To show that the helical spin state is possible, we discuss the spin structure of this compound using the approach that was used to explain the spiral magnetism of $\beta\text{-MnO}_2$.⁵⁶ In the present compound, three exchange interactions between the FeBr_4 anions, J_1 , J_2 , and J_3 , as illustrated in Figure 10a, are taken into account. J_1 represents the exchange interaction

between two neighboring anions along the a -axis, whereas J_2 and J_3 are long-range interactions along the b - and c -axes, respectively, mediated by the donor π -electron system through $\text{TTF}-\text{Br}\cdots\text{Br}-\text{Fe}$ contacts. Assuming that these interactions are isotropic and depend only on the intersite vectors between the two spins (\mathbf{R}_{ij}), the total exchange interaction energy is expressed as

$$E \cong -J(\mathbf{Q})S^2$$

$$J(\mathbf{Q}) = \max_{\mathbf{q} \in \text{BZ}} J(\mathbf{q}) = \max_{\mathbf{q} \in \text{BZ}} \sum_{\langle ij \rangle} J_{ij}(\mathbf{R}_{ij}) \exp(-\mathbf{q} \cdot \mathbf{R}_{ij}) \quad (4)$$

where only the largest Fourier component of the exchange interaction $J(\mathbf{Q})$ in the first Brillouin zone (BZ) is taken into account. If we focus on one FeBr_4^- anion, this anion is connected to two neighboring anions with $\mathbf{R}_{ij} = (\pm 1/2, 0, 0)$ with the exchange interaction J_1 . For the next-neighboring interaction J_2 , there are two different types of sites, namely, $\mathbf{R}_{ij} = (0, \pm 1/2, \pm 1/2)$ and $(\pm 1/2, \pm 1/2, \pm 1/2)$. For the former sites, each anion is connected to the anion at the origin with two equivalent interaction paths expressed as J_2 , whereas for the latter group only one interaction path connects anions. For the interaction J_3 , the neighboring sites are $\mathbf{R}_{ij} = (0, 0, \pm 1)$ and $(\pm 1/2, 0, \pm 1)$, and both of them have coordination numbers of eight. As a result, the Fourier component $J(\mathbf{q})$ for the wave vector $\mathbf{q} = (q_a, q_b, q_c)$ is expressed as

$$J(\mathbf{q}) = 2J_1 \cos\left(\frac{q_a}{2}\right) + 8J_2 \cos\left(\frac{q_b}{2}\right) \cos\left(\frac{q_c}{2}\right) + 8J_2 \cos\left(\frac{q_a}{2}\right) \cos\left(\frac{q_b}{2}\right) \cos\left(\frac{q_c}{2}\right) + 8J_3 \cos(q_c) + 8J_3 \cos\left(\frac{q_a}{2}\right) \cos q_c \quad (5)$$

Figure 10b gives the wave vector \mathbf{Q} (the wave vector \mathbf{q} that maximizes $J(\mathbf{q})$) for given values of the exchange interactions J_2 and J_3 normalized with $|J_1|$. There are two regions that stabilize helical-order states with the wave vectors $\mathbf{Q} = (\pi, 0, q_c)$ (shaded region) and $(0, 0, q_c)$ (hatched region), where $q_c = 2 \cos^{-1}(|J_2/2J_3|)$ corresponds to the helical pitch. It should be noted that in both cases the helical alignment is realized by the presence of the exchange interactions J_2 and J_3 , which are mediated by the π -electron layer. Therefore, the complex magnetic behavior observed in this salt is also the consequence of the π -d interaction originating from the intermolecular halogen \cdots halogen contacts.

Effect of the π -d Interaction on the Magnetoresistance.

In this section, the role of the interplay between the π - and d-electrons from the magnetoresistances (MR) of the FeCl_4 salt is discussed. The MR of this salt shows complicated behaviors, whose peculiarities are summarized as follows: (i) In the low-field region there exist two stepwise increases in MR at $B_1 \sim 1$ T and $B_2 \sim 2$ T whose fields increase as the pressure increases. (ii) In the field higher than B_2 and lower than ca. 10 T, MR decreases under low pressure (≤ 5 kbar) and increases under high pressure (≥ 9 kbar). (iii) Above 10 T, MR decreases regardless of pressure. (iv) Below 10 T, hysteresis of MR between the field-increasing and field-decreasing process is observed.

The magnetic field B_1 of the FeCl_4 salt is attributed to the spin-flop transition field of the π -electron spins $B_{\text{SF}-\pi}$, since

(56) Yoshimori, A. *J. Phys. Soc. Jpn.* **1959**, *14*, 807–821.

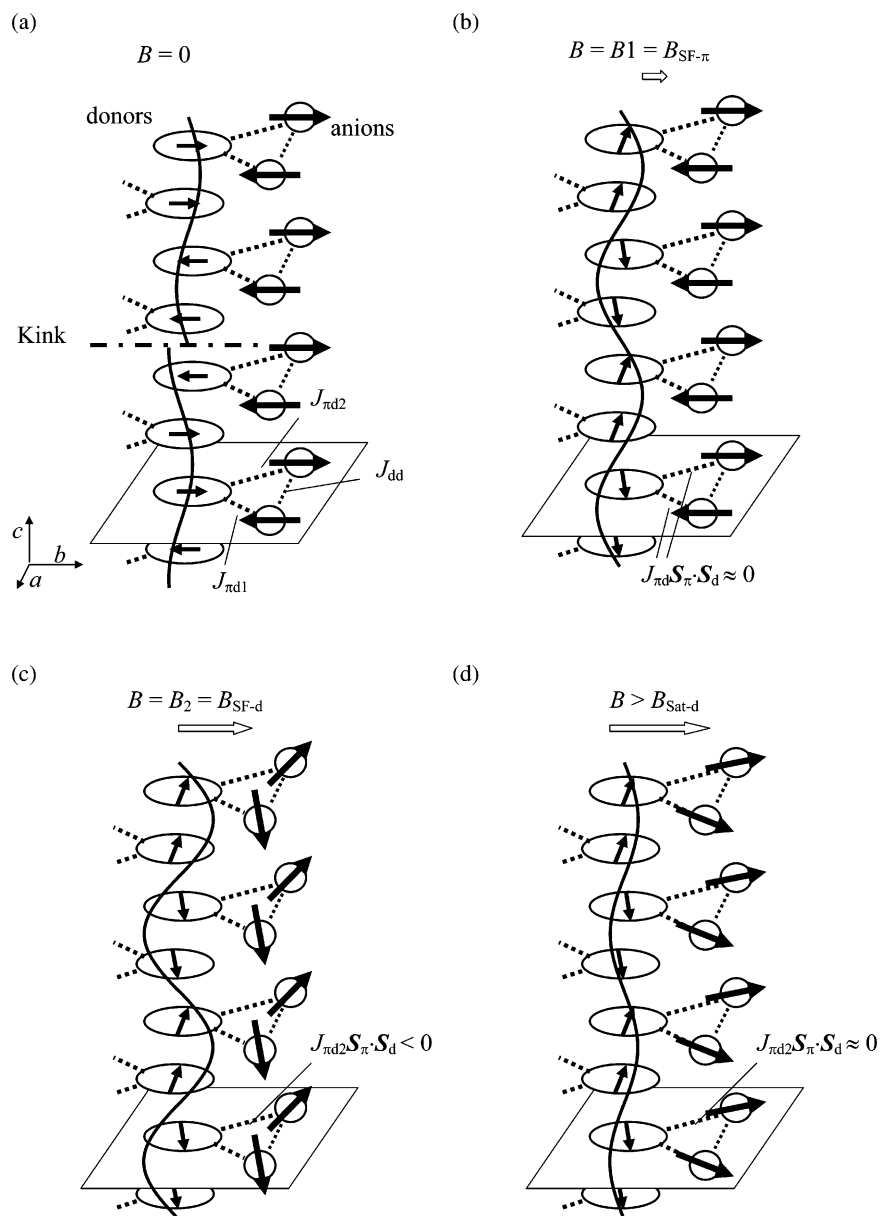


Figure 11. Spin structure model of the FeCl₄ salt under magnetic fields. (a) $B = 0$, (b) $B = B_{SF-\pi}$ (spin-flop field of the π -electron spins), (c) $B = B_{SF-d}$ (spin-flop field of the d-electron spins), and (d) $B = B_{Sat-d}$ (saturation field of the d-electron spins). Sinusoidal curves in each figure schematically depict the stability of the SDW on the donor column.

in a similar field a small anomaly in the MR of the GaCl₄ salt is observed ($B = 0.7$ T at 13 kbar, inset of Figure 8a) that suggests the spin-flop transition of the localized π -electron spins on the donor molecules. As the magnetization curve for $B \parallel b$ at 2 K shows a spin-flop transition at $B_{SF-d} \cong B_2 = 2$ T (Figure 4b), the leap in the MR at this field is a result of the spin-flop transition of the d-electron system. Finally, the saturation field of the FeCl₄ salt (B_{Sat-d}) is estimated at ca. 12 T as the field where the extrapolated magnetization curves reach $5 \mu_B$; hence, the steep decrease in MR corresponds to the saturation of the Fe³⁺ d-electron spins.

To explain the behavior of the MR for the FeCl₄ salt using these assignments for the anomalies, the following two points should be mentioned here. First, in the $2k_F$ SDW state for the three-quarter-filled electron system the spin density on the donor column has a periodicity of four molecules.

Namely, the π -electron spins inside a column are schematically expressed as $\cdots\uparrow\cdots\uparrow\cdots\downarrow\cdots\downarrow\cdots$ configuration. Second, each donor molecule is in contact with two neighboring Fe³⁺ d-electron spins through two competing antiferromagnetic π -d interactions $J_{\pi d1}$ and $J_{\pi d2}$. Therefore, the donor-anion-anion three-spin system (inside the parallelograms in Figure 10) can be regarded as a frustrated system if the anion-anion exchange interaction J_{dd} is also taken into account.

Now the behavior of the MR for the FeCl₄ salt can be qualitatively elucidated as follows. Without external magnetic field (Figure 11a), the spin alignment in the donor column may consequently have kinks from this spin frustration, which leads to the destabilization of the SDW state. When the fields reach the spin-flop field of the π -electron system ($B_{SF-\pi}$, Figure 11b), the π - and d-electron spins become quasi-orthogonal and the π -d interaction term $J_{\pi d}\mathbf{S}_{\pi}\cdot\mathbf{S}_d$ approaches zero; hence, the stabilized SDW state causes the

sudden increase in resistivity. At the field of the spin-flop transition of the d-electron system ($B_{\text{SF-d}}$, Figure 11c), the π - and d-electron spins become antiparallel through $J_{\pi d2}$ ($|J_{\pi d2}| \geq |J_{\pi d1}|$). As the SDW state of the π -electron layer and antiferromagnetic state of the d-electron layer have the same spatial periodicity, the π -d interaction again stabilizes the SDW state, leading to the further increase in resistivity. Finally, the field reaches the saturation field of the Fe^{3+} d-electron spins ($B_{\text{Sat-d}}$) and the π - and d-electron spins become orthogonal again; hence, the stabilization caused by the π -d interaction $J_{\pi d2}$ decreases and the MR again decreases above this field.

The presence of the hysteresis in MR can also be explained using this mechanism. Since the magnetic transitions between thermodynamic phases are, in general, second-order transition without hysteresis, the origin of the observed hysteresis should be related to the metastable state at the zero field caused by the frustration $J_{\pi d1}$, $J_{\pi d2}$, and J_{dd} as explained above, which disappears under the field of 15 T. When the magnetic field decreases to less than $B_{\text{Sat-d}}$, the frustration appears again. However, as the frustration near the saturation field is very weak, the π -electron spins go back to the SDW state, having fewer kinks than before the application of the magnetic field; hence, the MR in the demagnetizing process is higher than that in the magnetizing process. Finally, the pressure dependence of the MR in the intermediate field region ($B_{\text{SF-d}} < B < B_{\text{Sat-d}}$) is explained as follows. As the applied pressure increases, the intermolecular distance decreases and the π -d interaction $J_{\pi d1}$, $J_{\pi d2}$ increases; hence, the frustration of the π - and d-electron spins becomes larger. As a result, the increase in MR caused by the disappearance of the frustration by applying the magnetic field becomes larger as the external pressure is higher.

Effect of the π -d Interaction on the ESR Spectra. We discuss the effect of the π -d interaction appearing on the ESR spectra. The results of ESR measurements for the FeX_4 salts are, at first glance, contradictory to the presence of the π -d interaction. Namely, a sharp signal from the π -electrons and a broad signal from the d-electrons are separately observed above $T = 30$ K. In general, these two signals should coalesce to give a single signal if an exchange interaction with a magnitude of $h\nu/k_B \sim 0.4$ K ($\nu = 9$ GHz for X-band ESR spectrometer) is present between the two spin systems. Semiempirical molecular orbital calculations using a PM5 Hamiltonian⁵⁷ give an explanation for this discrepancy. According to the calculations, the contributions of the Br 4p orbital to the HOMO of the neutral EDO-TTFBr₂ (X = Br) molecules are negligible (atomic orbital coefficient, 0.06), whereas a significantly greater contribution is observed for NHOMO (next-highest-occupied molecular orbital, atomic orbital coefficient: 0.17), as illustrated in Figure 12a. This result means that the π -d interaction is mainly mediated by the paired electrons in NHOMO, and the unpaired electron in the partially oxidized HOMO, which gives the sharp signal in the ESR spectra, is only responsible for the transport property and does not directly interact with

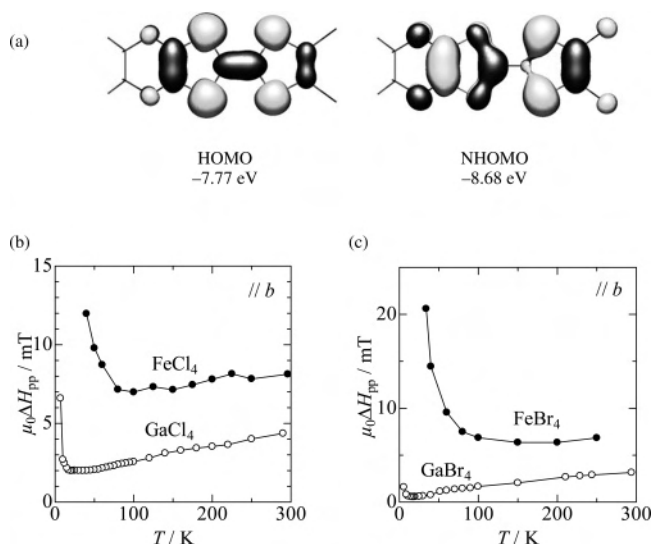


Figure 12. (a) HOMO (left) and NHOMO (right) of EDO-TTFBr₂ calculated using the PM5 Hamiltonian. (b) Temperature dependence of the ESR line width of the π -electron spins of the FeCl_4 and GaCl_4 salts under the applied field parallel to the b -axis. (c) Temperature dependence of the ESR line width of the π -electron spins of the FeBr_4 and GaBr_4 salts under the applied field parallel to the b -axis.

the d-electron spins. For the quantitative discussion, however, a higher level of calculation is necessary, in which the spin polarization effect caused by the partial oxidation of the donor molecule is taken into account.

Although there is a lack of coalescence of the signals from the π -electrons and d-electrons, the ESR line width of the FeX_4 salts suggests the presence of the π -d interaction even in the high-temperature range. For the GaX_4 salt, the ESR line width is expressed as $\Delta H_{\text{Ga}} \propto \tau_{\text{e-ph}}^{-1} + \tau_{\text{imp}}^{-1}$, where $\tau_{\text{e-ph}}$ and τ_{imp} are the electron-phonon relaxation time and the impurity-scattering relaxation time, respectively. For the FeX_4 salt, the line width becomes $\Delta H_{\text{Fe}} \propto \tau_{\text{e-ph}}^{-1} + \tau_{\text{imp}}^{-1} + \tau_{\text{mag}}^{-1}$, due to the contribution of the magnetic scattering by the counteranion. The magnetic scattering time τ_{mag} should therefore be proportional to the difference of the line widths between the FeX_4 and GaX_4 salts. Parts b and c of Figure 12 present the ESR line widths $\mu_0 \Delta H_{\text{pp}}$ of FeX_4 (narrow signal) and GaX_4 salts for the FeCl_4 - GaCl_4 and FeBr_4 - GaBr_4 pairs, respectively. The difference in $\mu_0 \Delta H_{\text{pp}}$ of the two signals shows little temperature dependence from room temperature down to ca. 70 and 150 K for the FeCl_4 - GaCl_4 and FeBr_4 - GaBr_4 pairs, respectively, below which point it begins to increase as the temperature decreases. As these temperatures correspond to the temperature where the magnetic susceptibilities of the FeX_4 salts begin to deviate from the Curie-Weiss law, we can conclude that the magnetic interaction between the anions affects the ESR signal of the conduction π -electrons, which indicates the presence of π -d interaction between the donor layer and anion layer.

Effect of the Oxygen-Substitution in the π -Donor Molecule. Finally, we compare the present results of the salts with oxygen-substituted donor molecule EDO-TTFBr₂ with those of the nearly isomorphous salts based on the all-sulfur analogue EDT-TTFBr₂.³⁸ In the EDT-TTFBr₂ salts, the

(57) Stewart, J. J. P. *MOPAC2002*; Fujitsu Limited: Tokyo, Japan, 2001.

ground state of the π -electron system is characterized as an antiferromagnetic state, due to the dimerization-induced Mott transition or the charge ordering, whereas the EDO-TTFBr₂ salts have SDW ground states. Comparison of the crystal structure by examination of oxygen-substitution reveals that the lattice parameters both along the π - π stacking direction ((EDT-TTFBr₂)₂FeBr₄, 7.066(10) Å; (EDO-TTFBr₂)₂FeBr₄, 6.997(4) Å) and along the direction of the side-by-side S \cdots S contacts ((EDT-TTFBr₂)₂FeBr₄, 13.10(2) Å; (EDO-TTFBr₂)₂FeBr₄, 12.670(4) Å) become slightly shorter, because of the smaller van der Waals radius of oxygen than that of sulfur and shorter bond distances of C–O than those of S–S. As a result, the intermolecular overlap integral of the EDO-TTFBr₂ salt is larger than that of the EDT-TTFBr₂ salt (p in Figure 1b: (EDT-TTFBr₂)₂FeBr₄, –29.8; (EDO-TTFBr₂)₂FeBr₄, –35.5). This difference decreases the ratio U/t in the EDO-TTFBr₂ salt, where U is the on-site Coulomb repulsion and t is the transfer integral (it is a good approximation that U has the same value for both compounds, for the HOMOs of EDT-TTFBr₂ and EDO-TTFBr₂ are mainly localized on the central TTF moiety). As a result, the π -electrons in the EDO-TTFBr₂ salts bear more itinerant character than those of the EDT-TTFBr₂ salts; thus, Mott transition or charge ordering is less favorable. Nevertheless, due to their quasi-1D character, the ground states of the π -electrons in the EDO-TTFBr₂ salts become SDW states. Another difference between the EDT-TTFBr₂ and EDO-TTFBr₂ salts is their ground state of the d-electron spins. The magnetic ground state of (EDT-TTFBr₂)₂FeBr₄ is a typical antiferromagnet, having Néel temperature $T_N = 11$ K. On the other hand the d-electron spins in (EDO-TTFBr₂)₂FeBr₄ show complicated stepwise anomalies at $T_N = 13.5$ K and $T_{C2} = 8.5$ K. Our model calculations described above suggest the importance of the exchange pathways J_2 and especially J_3 for the realization of the complex magnetic ground state such as helical spin alignment. In the EDT-TTFBr₂ salt, the magnitude of these exchange interactions is supposed to be weaker due to the localized nature of the π -electrons on the donor units. However, in the EDO-TTFBr₂ salt, the slightly delocalized π -electrons give larger exchange interaction between the d-electrons mediated by the π -electron layer, leading to the higher Néel temperature and complex magnetic ground state.

Summary

We have developed two π -d interaction-based conducting molecular antiferromagnets (EDO-TTFBr₂)₂FeX₄ (X = Cl, Br) and their reference compounds (EDO-TTFBr₂)₂GaX₄ without localized spins in the counteranions and investigated their crystal structure and physical properties. In the crystals of these isomorphous salts, the donor molecules are uni-

formly stacked to make quasi-1D columns. The most remarkable structural feature is the presence of close intermolecular TTF–Br \cdots X–Fe contacts between the donor columns and anion chains. These salts show metallic behavior at around room temperature and undergo an SDW transition in the low temperature confirmed with the ESR line width divergence of the GaX₄ salts. The resistivity of the FeCl₄ salt shows two anomalies due to the successive transitions of the π -electron layer and another anomaly coming from the long-range magnetic ordering of the FeCl₄ layer. The magnetic susceptibility of the FeX₄ salts shows the magnetic order of the d-electron spins, despite the absence of significant intermolecular contacts between magnetic anions. The FeCl₄ salt undergoes an antiferromagnetic transition at $T_N = 4.2$ K, whereas the FeBr₄ salt shows successive magnetic transitions at $T_N = 13.5$ K and $T_{C2} = 8.5$ K having a possible magnetic ground state with a helical spin structure created by the presence of the π -d exchange interaction through the donor layer. Although on the ESR spectra of the FeX₄ salts signals from the π - and d-electron spins are observed separately, the line width of the π -electron spins broadens in the temperature range where the susceptibility deviates from the Curie–Weiss behavior, showing the presence of π -d interaction. For the GaCl₄ salt, negative MR is observed in the low-field region, suggesting a decrease of the SDW gap by the application of the magnetic field. The MR of the FeCl₄ salt shows two abrupt increases, which proves the presence of field-induced successive transitions in the composite π -d spin system. The field dependence of the MR of this salt can be qualitatively explained based on the frustrated magnetic structure of π - and d-electron spins interacting with each other using the π -d and d-d interactions. In conclusion, the introduction of the halogen \cdots halogen interaction to the molecular conducting magnet is a useful methodology not only from the viewpoint of crystal engineering but also for the realization of a novel magnetic system based on the π -d interaction through the close halogen \cdots halogen intermolecular contacts between the conducting π -electron system and the magnetic d-electron system.

Acknowledgment. This work was financially supported by Grant-In-Aid for Scientific Research (Nos. 12046231, 14540530, and 15073211) from the Ministry of Education, Science, Sports, and Culture, Japan.

Supporting Information Available: Full bond lengths and angles, atomic coordinates, and complete crystal structure results are given in CIF format. This material is available free of charge via the Internet at <http://pubs.acs.org>.

IC061871Y